

# Visco-plasticity during In-situ Cooling from Solidification of a Nickel-Base Single Crystal Superalloy using Neutron Diffraction

D'Souza, Neil; Kelleher, Joe; Kabra, Saurabh; Panwisawas, Chinnapat

DOI:

[10.1016/j.msea.2016.11.013](https://doi.org/10.1016/j.msea.2016.11.013)

License:

Creative Commons: Attribution-NonCommercial-NoDerivs (CC BY-NC-ND)

Document Version

Peer reviewed version

Citation for published version (Harvard):

D'Souza, N, Kelleher, J, Kabra, S & Panwisawas, C 2017, 'Visco-plasticity during In-situ Cooling from Solidification of a Nickel-Base Single Crystal Superalloy using Neutron Diffraction', *Materials Science and Engineering A*, vol. 681, pp. 32-40. <https://doi.org/10.1016/j.msea.2016.11.013>

[Link to publication on Research at Birmingham portal](#)

## Publisher Rights Statement:

Checked for eligibility: 04/11/2016

## General rights

Unless a licence is specified above, all rights (including copyright and moral rights) in this document are retained by the authors and/or the copyright holders. The express permission of the copyright holder must be obtained for any use of this material other than for purposes permitted by law.

- Users may freely distribute the URL that is used to identify this publication.
- Users may download and/or print one copy of the publication from the University of Birmingham research portal for the purpose of private study or non-commercial research.
- User may use extracts from the document in line with the concept of 'fair dealing' under the Copyright, Designs and Patents Act 1988 (?)
- Users may not further distribute the material nor use it for the purposes of commercial gain.

Where a licence is displayed above, please note the terms and conditions of the licence govern your use of this document.

When citing, please reference the published version.

## Take down policy

While the University of Birmingham exercises care and attention in making items available there are rare occasions when an item has been uploaded in error or has been deemed to be commercially or otherwise sensitive.

If you believe that this is the case for this document, please contact [UBIRA@lists.bham.ac.uk](mailto:UBIRA@lists.bham.ac.uk) providing details and we will remove access to the work immediately and investigate.

# Visco-plasticity during In-situ Cooling from Solidification of a Nickel-Base Single Crystal Superalloy using Neutron Diffraction

Neil D'Souza<sup>1</sup>, Joe Kelleher<sup>2</sup>, Saurabh Kabra<sup>2</sup>, Chinnapat Panwisawas<sup>3\*,\*</sup>

<sup>1</sup>Rolls-Royce plc, PO Box 31, Derby, DE24 8BJ, UK

<sup>2</sup>ISIS Neutron and Muon Source, Science and Technology Facilities Council, Rutherford Appleton Laboratory, Harwell, Oxford, Didcot OX11 0QX, UK

<sup>3</sup>School of Metallurgy and Materials, University of Birmingham, Birmingham B15 2TT, UK

*\*Corresponding author: c.panwisawas@bham.ac.uk*

## Abstract

In-situ neutron diffractometry is performed to study the visco-plasticity in a nickel-base single crystal superalloy during in-situ cooling from high temperatures. It is found that visco-plastic deformation has two contributions from creep and stress relaxation, which are subject to the accumulation of dislocation activity and dislocation annihilation, respectively. Use has been made of the lattice strain evolution of the (200)  $\gamma + \gamma'$  peak to confirm this effect. The decrease in lattice strain and macro-stress during in-situ cooling has been observed and confirms that there was softening taking place before thermal strain dominates at lower temperatures. Therefore, in-situ isothermal cyclic loading and relaxation tests under strain control, akin to thermal contraction during casting, have been carried out. A visco-plasticity law was then developed based on macro-strain development during creep and lattice strain evolution during stress relaxation within an appropriate timescale, where transient effects are captured. The constitutive law developed has been used to independently determine the

evolution of stress and strain during in-situ cooling. The implementation of these findings into thermo-mechanical modelling during cooling from solidification is also discussed.

**Key words:** neutron diffraction; in-situ cooling; visco-plasticity; stress relaxation; lattice strain

## 1. Introduction

Mechanical response during the investment casting of single-crystal superalloys is governed by the thermo-mechanical histories induced by mechanical deformation arising from differential thermal contractions of the metal (superalloy) and ceramic (mould and internal core), under casting conditions [1, 2]. Cooling rates [3] and dendritic growth rates [4, 5] can be controlled through optimising the furnace parameters and appropriate component design to minimise defects in single-crystal castings that also conform to acceptable dimensional tolerance. On cooling during and after solidification of a single crystal superalloy casting, little is known about the in-situ introduction of high temperature deformation [6, 7] and the quantification of processing-induced deformation [8]. To the best of the authors' knowledge, finite element calculations that determine thermo-mechanical behaviour are traditionally contingent on the quality of the as-cast materials data and thermo-physical properties used in the model [9]. Such an approach has advantages, as it confers a predictive capability on turbine blade designers enabling them to produce a design space for achieving a minimal-waste manufacturing route and design criteria with functional integrity.

Processing-induced plasticity can be introduced at temperatures close to the  $\gamma'$  solvus temperature in single crystal Ni-base superalloys [10 - 12]. In that study it was proposed that 2 – 3 % plasticity induced at high temperatures leads to a dislocation network [1], which

results in re-crystallisation during subsequent solution heat treatment to release the stored strain energy within the microstructure. Typical mechanisms resulting in a reduction in the dislocation density include creep and stress relaxation [13 - 19]. On the other hand, larger stresses arising at lower temperatures can lead to other commonly encountered casting defects, such as hot tears [20, 21]. For a prediction of such casting defects, it becomes challenging to address how processing-induced plasticity should be quantitatively treated on the one hand, as well as whether time-dependent plasticity should also be considered [1]. The latter is important, since it is accompanied by relaxation and reduction in the stress and which is dependent on the time that the casting resides in the critical temperature regime during cooling [3].

Materials modelling used in thermo-mechanical analysis follows usually plastic flow (time independent) or visco-plastic flow (time dependent) approaches, the applicability of which depends upon the working temperature regimes [22, 23]. Within process modelling of investment casting, owing to the limited high temperature materials data, the extrapolation of intermediate temperature tests permits the elasto-plastic analysis to be performed. Uniaxial tensile or compression testing using constant strain rate at elevated temperatures is conventionally carried out to derive the empirical or phenomenological laws for plastic flow for use in this analysis [1]. However, the predictive capability can be further improved by taking into account visco-plasticity [3]. Visco-plasticity is conventionally incorporated through consideration of secondary (steady state) creep testing using constant stress at elevated temperature. Although creep has technological significance [24 - 28] and offers a convenient means of including visco-plasticity in the analysis, it is not altogether relevant to investment casting process modelling. The principal objections here are related to the material condition, i.e. as-cast, segregated and not homogenous, but also the fact that visco-

plastic behaviour has to be considered at small time scales to accurately capture the stress/strain transients during cooling, i.e. few minutes as compared to hours [3].

On the other hand, advent of in-situ testing capabilities equipped with synchrotron [29, 30] or neutron [31, 32] light sources provide substantial benefits for the observation of lattice strain evolution, which dictates the underlying macroscopic response at the component level. Following such an approach, the aim in this study is therefore three-fold.

First, neutron diffraction experiments are used to investigate the processing-induced visco-plasticity during the in-situ cooling of uniaxial tensile samples under representative casting conditions. Towards this end, the strain control mode was employed, where the length of the sample is fixed during cooling, which is akin to metal freezing around a rigid (immovable) ceramic core. As mentioned before, to capture the transients in stress/strain during cooling it is required to use a small neutron data acquisition time, but without compromising the error in strain measurement. Our previous work [31] has used 10 mins acquisition time; however more recently a lower acquisition time of 3 mins has been observed to be statistically reliable [32]. Additionally, from the measurement of macro-stress a key insight will be obtained on the efficacy of this choice of lower acquisition time, as the micro-strain directly measured using diffraction can be compared with the macro-strain deduced from the stress.

Second, isothermal relaxation testing is carried out to rationalise the visco-plasticity and stress relaxation behaviour at 950°C and 1000°C, and corresponds to the temperature range of the cooling experiments. Using the discrete data, best-fit equations for creep and stress relaxation can be obtained to quantify the visco-plasticity over the stress and temperature range, which is akin to the creep modelling approach that has been conventionally adopted [1 – 3]. Using these equations the visco-plasticity can be calculated during cooling and

subsequently compared with the experimentally measured values. The rationalisation of process-induced visco-plasticity during cooling from solidification is then discussed.

One criticism for such an approach is that during solidification and subsequent cooling, alloys might not have not reached kinetic equilibrium and  $\gamma/\gamma'$  might not possess a good coherent relationship. It has been however demonstrated that  $\gamma'$  precipitation kinetics is diffusion controlled and therefore accompanied by interfacial equilibrium [33]. Consequently, the coherency is unaffected, as this is determined by the interfacial composition. On the other hand, the other important drawback of using isothermal creep/relaxation tests to determine visco-plasticity is to ignore the history dependence of the prior deformation existing within the solid, as it has cooled to the given temperature. One possible way of taking this into account was by adopting the cyclic relaxation tests, where the deformation in prior cycles is incorporated within the relaxation tests. Therefore, a third and important objective is to assess the validity of using isothermal loading tests by re-heating to calculate visco-plasticity. This is achieved by directly comparing the experimentally measured visco-plastic strain in the in-situ cooling experiments to that predicted using the relaxation/creep tests.

Implications of this work will be beneficial for establishing a better mesoscopic description for the process modelling of investment casting by examining the conditions in which this approach can be adopted.

## **2. Method**

### **2.1 Material**

Tensile test pieces with a diameter of 5.85 mm and a gauge length of 29 mm of CMSX4 (nominal composition in Table 1) following the design used in [31], have been fabricated

using the state-of-the-art investment casting process at the Precision Casting Facility (PCF), Rolls-Royce plc, Derby, UK. Prior to casting, moulds were seeded with the required orientation to ensure an axial orientation of the single crystals to within  $5^\circ$  from [100]. The single crystals were then directionally solidified in a small-bore furnace using a withdrawal rate of  $5 \times 10^{-5}$  m/s. In this manner, the orientation of the seed was conferred on to the test pieces that subsequently solidified; more details are included in [31]. Tensile bars were subject to electro-discharge machining (EDM) at the shoulders and grips, but the gauge length portion remained in the as-cast condition.

## **2.2 Neutron diffraction measurement**

A series of samples were examined during in-situ heating, loading and subsequent relaxation of stress on the ENGIN-X instrument, at the ISIS pulsed neutron facility, Rutherford Appleton Laboratory, Didcot, UK. An optical furnace was used to heat the samples in air and a K-type thermocouple was held in contact with the sample to monitor temperature profiles. Isothermal stress relaxation tests were conducted at two temperatures,  $950^\circ\text{C}$  and  $1000^\circ\text{C}$ . The samples were heated at a ramping rate of  $10^\circ\text{C}/\text{min}$  up to  $800^\circ\text{C}$  and thereafter at a rate of  $5^\circ\text{C}/\text{min}$  to the set temperatures. Prior to loading, each sample was held at the requisite testing temperature for nine minutes for thermal equilibrium and also to get the extensometer stabilised. At each temperature, a range of initial tensile stresses were used for stress relaxation testing and the stresses were applied at a rate a strain rate of  $0.2\% \text{ min}^{-1}$ . Specifically, the loading started with a relatively small stress and dwelt at the stress for nine minutes under load control, which was then followed by stress relaxation under strain control mode for an additional 12 minutes. The initial stress was then increased by an increment of 10 MPa from the previous applied stress before another dwelling and stress relaxation test was conducted. The predicted stress ranges derived from a previous modelling study of

solidification and cooling of simple one-dimensional and three-dimensional bobbin-type geometries has been taken as a reference for the selection of the initial stress for each temperature [2, 3].

The loading axis in these experiments was horizontal and at  $45^\circ$  to the incident beam, allowing simultaneous measurement of lattice spacing both parallel and perpendicular to the loading axis. The samples were mounted such that the stress was applied along specimen axis. The positioning of the rig was such as to yield the longitudinal lattice spacing in one detector and the transverse lattice displacement in the other. The detectors were fixed at  $90^\circ$  to the incident beam and the data are obtained from the full  $\pm 15^\circ$  detector bank [31]. In all cases the neutron measurement volume was typically of the order of few cubic mm [34]. For the single crystal to be correctly aligned measurements are taken and the sample subsequently rotated until the desired lattice planes, in this (100) and (010), are located in the north-bank and south-bank detector respectively. At time-of-flight sources, such as ISIS, neutron pulses each with a continuous range of velocities and therefore wavelengths are directed at a specimen. The flight times of diffracted neutrons are measured and the wavelengths are then calculated. In Ni-base alloys, since  $\gamma$  (A1) and  $\gamma'$  (L1<sub>2</sub>) have almost identical lattice parameters, any fundamental reflection obtained in the experiment are produced from both phases. However, since  $\gamma'$  possesses an ordered structure primitive cubic lattice, additional super-lattice reflections are also observed. Thus the position of the first-order (100) [(hkl), where h, k and l are mixed] can be determined unequivocally, from which the (200)  $\gamma + \gamma'$  doublet peak can be fitted using a constrained double peak fit [34]. The doublet analysis was carried out using routines written in the OpenGenie software with the appropriate peak shape [35].

### **2.3 Data analysis**



In the current study, the stress relaxation tests were carried out under strain-control mode. The elastic (lattice) strain,  $\varepsilon^{\text{el}}$ , during stress relaxation could be calculated using the following equation:

$$\varepsilon^{\text{el}} = (d - d_0)/d_0 \quad (1)$$

where  $d_0$  is the stress-free lattice spacing and  $d$  is the lattice spacing at any instant under load. With neutron diffraction, both the  $d$ -spacing for (100) crystal planes of  $\gamma'$  ( $L1_2$ ) ( $d_{100}$ ) and that for (200) crystal planes of ( $\gamma + \gamma'$ ) ( $d_{200}$ ) could be identified. The stress relaxation tests lasted 12 mins and the data acquisition time was 3 mins (i.e.,  $\Delta t = 0, 3, 6, 9$  and 12 mins). By calculating the relaxation strain,  $\varepsilon^{\text{rel}}$  for different durations, under different temperatures and stress levels, it is possible to derive the dependence of strain rate (or strain) on temperature, stress time and microstructure. The strain rate equation is anticipated to be in the form;

$$\dot{\varepsilon}^{\text{rel}} = \dot{\varepsilon}^{\text{rel}}(t, T(t), \sigma, \boldsymbol{\mu}) \quad (2)$$

Here,  $\boldsymbol{\mu}$  is referred to microstructural parameters [24, 25, 28], which is not considered for now. The experimental data is to be fitted using a power law equation for the stress and strain development during relaxation and within a time interval of up to 12 mins;

$$\dot{\varepsilon}^{\text{rel}}(T) = A_0 \exp\left(-\frac{Q}{RT}\right) \left(\frac{\sigma}{\sigma_0}\right)^n t^m$$

where  $A = A(T) = A_0 \exp\left(-\frac{Q}{RT}\right)$ ,  $n = n(T)$  and  $m = m(T)$  are temperature dependent. In addition to in-situ isothermal testing, in-situ cooling tests were also performed for two different initial stresses of 350 MPa and 280 MPa, respectively. The sample was heated from room temperature to 1000°C and following an isothermal hold for 9 mins. A tensile stress was then applied and the sample was held for another 9 mins under load control prior to cooling. Cooling was carried out at a nominal rate of 1 °C min<sup>-1</sup>. For this test, the sample was

held under strain control mode to simulate the real strain development during casting. During casting, the metal solidifies and cools in a ceramic mould and hence contraction of metal around a rigid ceramic will place the metal in a state of tension [1]. This is similar to what occurs in the cooling experiment performed under strain control, where the contraction of the sample is severely constrained by the Instron grips. The initially applied stresses of 350 MPa and 280 MPa are equivalent to the range of stresses that would have developed in the metal during solidification down to 1000°C [2, 3].

The experimental conditions of cooling under an initially applied axial load lend itself to an elementary one-dimensional analysis, from which the stress and strain development during cooling can be calculated;

$$\varepsilon = \varepsilon^{\text{th}} + \varepsilon^{\text{el}} + \varepsilon^{\text{vp}}$$

$$\sigma = E\varepsilon^{\text{el}}$$

$$\varepsilon^{\text{th}} = \alpha(T - T_{\text{ref}})$$

$$\varepsilon^{\text{vp}} = \int_0^{\Delta t} \frac{d\varepsilon^{\text{vp}}}{dt} dt$$

Here,

$$\Delta\varepsilon = \Delta\varepsilon^{\text{th}} + \Delta\varepsilon^{\text{el}} + \Delta\varepsilon^{\text{vp}}, \quad (3)$$

where  $\alpha$  is the thermal expansion coefficient,  $\Delta\varepsilon$  is the change in strain during cooling from  $T$  to  $[T - \Delta T]$  in time interval  $\Delta t$  ( $\Delta T > 0$ ) and  $\Delta\varepsilon^{\text{vp}}$  is the visco-plastic strain. For un-restrained (free) contraction,  $\Delta\varepsilon = \alpha \Delta T$  and therefore,  $\Delta\sigma = 0$ . However, for complete constraint  $\Delta\varepsilon = 0$  and for all other cases,  $\Delta\varepsilon > 0$ . Since the cooling was done in the strain-control mode,  $\Delta\varepsilon = 0$  and Equation 3 can be modified as;

$$|\Delta\varepsilon^{\text{th}}| - |\Delta\varepsilon^{\text{el}}| = |\Delta\varepsilon^{\text{vp}}|, \quad (4)$$

where  $\Delta\varepsilon^{\text{th}} = \alpha\Delta T$  and  $\Delta\varepsilon^{\text{el}} = \frac{\Delta\sigma}{E}$ . Therefore, from the experimentally measured  $\Delta T$  and  $\Delta\sigma$ , the incremental visco-plastic strain during cooling between successive temperature intervals can be calculated, where  $\alpha = 15 \times 10^{-6} \text{ K}^{-1}$  in the temperature range [3].

### 3. Results

#### 3.1 Stress build-up and visco-plasticity during continuous cooling

Figure 1 presents the evolution of stress with temperature during continuous cooling at a nominal cooling rate of  $1^\circ\text{C}/\text{min}$ , where the initial stresses were,  $\sigma_i = 350 \text{ MPa}$  (Figure 1(a)) and  $280 \text{ MPa}$  (Figure 1(b)), respectively. The measurement uncertainty in the measured stress over the range of stresses considered in these experiments was  $1160 \text{ Pa}$  (i.e.  $0.35\%$  of the applied load, which was in the range of  $7.5 \text{ kN}$  to  $12 \text{ kN}$ ). In the first instance cooling was carried in the temperature range,  $900^\circ\text{C} \leq T \leq 998^\circ\text{C}$  and in the latter;  $950^\circ\text{C} \leq T \leq 996^\circ\text{C}$ . The initial stages of cooling were accompanied by a decrease in stress. For  $\sigma_i = 350 \text{ MPa}$ , stress decreases continuously by up to  $105 \text{ MPa}$  within  $15 \text{ mins}$  corresponding to the temperature range,  $984^\circ\text{C} \leq T \leq 998^\circ\text{C}$ . Whereas  $\sigma_i = 280 \text{ MPa}$ , stress decreases continuously by up to  $9 \text{ MPa}$  within  $6 \text{ mins}$  corresponding to the temperature range,  $990^\circ\text{C} \leq T \leq 996^\circ\text{C}$ . On further cooling, for  $\sigma_i = 350 \text{ MPa}$ , stress remains nearly constant over the following  $24 \text{ mins}$  corresponding to the temperature range,  $984^\circ\text{C} \leq T \leq 957^\circ\text{C}$  and thereafter monotonically increases up to  $900^\circ\text{C}$  (termination of test). As for  $\sigma_i = 280 \text{ MPa}$  stress increases continuously (although there is one instance of local relaxation at between  $974$  and  $976^\circ\text{C}$ ) up to  $950^\circ\text{C}$  (termination of test).

Figure 2 plots the visco-plastic strain calculated from the change in stress, i.e.  $\frac{\Delta\sigma}{E} = \Delta\epsilon^{el}$  with temperature during cooling and corresponding to an initial stress of 350 MPa. On the other hand, the elastic strain can also be measured directly from the axial (200)  $\gamma + \gamma'$  micro-strain by making use of the stress-free lattice spacing at the given temperature. The visco-plastic strain in both cases is then calculated using Equation 4 and is also included in Figure 2 and corresponding to the temperature range,  $970^\circ\text{C} \leq T \leq 1000^\circ\text{C}$ . The contribution of the uncertainty corresponding to the measured stress and the (200) lattice strain has also been indicated. The uncertainty for the (200) lattice strain,  $\Delta\epsilon(200) = (\Delta d_{200} / d_{200})$ , where  $\Delta d_{200}$  is the error in measurement of the (200) lattice spacing. It can be observed that there is very good agreement between the visco-plastic strains calculated using either approach, even after considering measurement uncertainty. This therefore implies that,  $\frac{\Delta\sigma}{E} = \Delta\epsilon^{el,macroscopic} \cong \Delta\epsilon^{200}$ . The good agreement between the macroscopic strain and the axial (200) lattice strain arises since the axial orientation of the samples was within  $5^\circ$  from [100]. This implies that (100) and (200) planes are near-normal to the applied axial stress. It follows importantly therefore that it is appropriate to treat the (200) fundamental  $\gamma + \gamma'$  peak as a composite peak in the analysis without the need for de-convolution of  $\gamma$  from  $\gamma'$  in (200). This aspect has been also demonstrated in our previous studies [31].

The evolution of stress and strain during cooling was examined within a wide range of applied stresses, ( $\sigma/\sigma_0 > 1$  and  $\sigma/\sigma_0 < 1$ ). Accordingly, Figures 3(a) and 3(b) present the calculated visco-plastic strain with temperature during cooling and corresponding to initial stresses of 350 MPa and 280 MPa respectively within the nominal temperature range,  $950^\circ\text{C} < T < 1000^\circ\text{C}$ . The following observations can be made and tabulated in Table 2. As for  $\sigma_i = 350$  MPa, visco-plasticity is accompanied by a decrease in stress of 77 MPa within 6 mins in the range,  $994.5^\circ\text{C} \leq T \leq 998^\circ\text{C}$ , where  $\Delta\epsilon^{vp} = 4 - 6 \times 10^{-4}$ . Thereafter,  $\Delta\epsilon^{vp} \approx 1 - 2 \times 10^{-4}$  for

a further 9 mins in the range,  $984^{\circ}\text{C} \leq T < 994.5^{\circ}\text{C}$ . During the constant stress region thereafter corresponding to a further time interval of 24 mins in the range,  $957^{\circ}\text{C} \leq T < 984^{\circ}\text{C}$ , there is a near ten-fold decrease in visco-plastic strain and  $\Delta\epsilon^{\text{vp}} = 0.6 - 0.9 \times 10^{-4}$ . On further cooling in the range,  $900^{\circ}\text{C} \leq T < 957^{\circ}\text{C}$ , the stress (and elastic strain) begins to increase. While  $\sigma_i = 280$  MPa, visco-plasticity is accompanied by an initial decrease in stress of 9 MPa within 6 mins in the range,  $990^{\circ}\text{C} \leq T \leq 996^{\circ}\text{C}$ , where  $\Delta\epsilon^{\text{vp}} \approx 10^{-4}$ . Even though the measurement uncertainty is half of the measured visco-plastic strain, thereafter during subsequent cooling in the range,  $950^{\circ}\text{C} \leq T \leq 990^{\circ}\text{C}$  visco-plasticity can be neglected and accompanied by increasing stress. However, some visco-plasticity is observed in a small temperature interval  $974^{\circ}\text{C} \leq T \leq 976^{\circ}\text{C}$ , where  $\Delta\epsilon^{\text{vp}} \approx 8 \times 10^{-5}$ . It is not clear for the exact reason for this. A possible reason is the operation of a recovery mechanism, with the decrease in elastic strain related to release of accommodation stress (also referred to as back-stress) and as observed in the creep experiments of Coakley *et. al.* [36]. However, in this analysis it must be emphasised that no attempt was made to separate out  $\gamma$  and  $\gamma'$  contribution in the (200) peak, as would be required for a detailed analysis of the micro-mechanism(s) involved.

### 3.2 Stress relaxation and creep strain from isothermal tests

Stress relaxation over a wide range of stresses was carried out under strain-control mode at two representative temperatures of  $950^{\circ}\text{C}$  and  $1000^{\circ}\text{C}$  respectively. The initial stresses were 340 MPa and 280 MPa respectively with an increment of 10 MPa and the measured lattice strain case corresponds to the composite (200)  $\gamma + \gamma'$  peak. Since the strain is dependent on the stress and testing temperature, for a meaningful comparison at two different temperatures and stresses, the initial applied stress has been normalised by the 0.2% yield stress,  $\sigma_0$  at that temperature, i.e.  $\sigma/\sigma_0$ . According to Equation 1, the evolution of lattice strain as a function of stress can be calculated as shown in Figure 4. In Figure 4, the measurement uncertainty has

not been included for each measurement to retain clarity in the figure. In summary, the range of measurement uncertainty for (200) lattice strain was  $30 \times 10^{-6}$  to  $45 \times 10^{-6}$  and  $35 \times 10^{-6}$  to  $60 \times 10^{-6}$  corresponding to the isothermal relaxation tests at 950°C (Figure 4(a)) and at 1000°C (Figure 4(b)) respectively.

Figure 5 then presents the evolution of lattice strain rate with  $\sigma/\sigma_0$  covering a range of some typical stresses and corresponding to temperatures of 950°C (Figure 5(a)) and 1000°C (Figure 5(b)), and included is the contribution of the measurement uncertainty in the (200) lattice strain. At each temperature the extent of stress relaxation is significantly dependent on the initial stress level. The higher the initial stress, the more pronounced the stress relaxation. The data acquisition time for each neutron measurement was 3 mins and therefore the lattice strain has been averaged over that time interval. For a given  $\sigma/\sigma_0$  and temperature, the strain rate decreases beyond  $\Delta t = 6$  mins. However, the temporal dependence for the relaxation strain rate is only prominent at 1000°C and for  $\sigma/\sigma_0 > 0.92$ .

Since the relaxation strain rate at 950°C is nearly constant for  $\sigma/\sigma_0 < 1$  over the entire time interval ( $\Delta \epsilon^{\text{rel}} < 10^{-6}$ ), a power law fit can be applied to obtain a best-fit for the experimental data and is given in Table 3. It is clear that in this case the temporal dependence is absent, i.e.  $m = 0$ . At 1000°C there exists a temporal dependence of strain rate for  $\sigma/\sigma_0 \gg 0.92$ . Also, in the continuous cooling experiments the data acquisition time for each measurement is 3 mins. Therefore, a power law fit is applied to obtain a best-fit for the strain rate relaxation with  $\sigma/\sigma_0$ , but for  $\Delta t = 3 \text{ mins}$  only at 1000°C. Therefore for such a best-fit,  $m = 0$ , since the data is acquired over the time interval of 3 mins. A similar best-fit can be obtained for time intervals of 6 mins, 9 mins and 12 mins, but relaxation in these time intervals have little physical significance with regards to the cooling experiments, as the

transient stresses and strains will not be captured. Consequently for  $\sigma/\sigma_0 < 1$ , the fitting parameters for  $\dot{\epsilon}^{\text{rel}}$  are tabulated in Table 3.

On the other hand, at higher temperatures, creep strain can also become dominant. The creep strain rate can be directly obtained from the isothermal hold at peak stress prior to relaxation (see Section 2.2). Figures 6(a) and 6(b) plot the creep strain rate over the 9 mins isothermal hold with  $\sigma/\sigma_0$  and referring to 950°C and 1000°C respectively. At each temperature the creep strain rate is dependent on the initial stress and increases with  $\sigma/\sigma_0$  and temperature. At 1000°C, the creep rate is 5 – 10 times greater than at 950°C for a given  $\sigma/\sigma_0$ . The temporal dependence for the creep strain rate is only prominent at 1000°C and for  $\sigma/\sigma_0 > 0.92$ . Like in the case of stress relaxation, a best-fit power law curve can be applied to the creep rate and the following fitting parameters are given in Table 3.

### **3.3 Contribution of stress relaxation and creep strain rate to visco-plasticity during cooling**

The relaxation or creep strain within a temperature interval,  $\Delta T$  (or time interval  $\Delta t$ ) can be calculated using the data in Table 3 as follows;

$$\Delta \epsilon^{\text{rel/creep}} = A \left[ \frac{\sigma(T) + \sigma(T - \Delta T)}{2\sigma_0(T)} \right]^n \Delta t \quad (5)$$

It is difficult to fit an Arrhenius type equation for the relaxation/creep strain rate over the entire temperature interval because at least three temperatures are required. Therefore, using a conservative approach the relaxation/creep strains calculated at 1000°C will be applied over the temperature interval of  $980^\circ\text{C} \leq T \leq 1000^\circ\text{C}$  and that calculated at 950°C will be applied over the temperature interval of  $950^\circ\text{C} \leq T \leq 960^\circ\text{C}$ . Implications of using such an approach will be presented in the discussion section. Accordingly, the calculated relaxation/creep strains in these temperature intervals are superimposed on the measured visco-plastic strain

in Figures 7(a) and 7(b) corresponding to the continuous cooling experiments,  $\sigma_i = 350$  MPa and  $\sigma_i = 280$  MPa respectively. In the case of the measured visco-plastic strain, the contribution of the uncertainty in measurement of the (200) lattice strain has been included. On the other hand, in the case of the calculated relaxation strain, the measurement uncertainty has been taken into consideration in obtaining the best-fit curve in Figure 5.

In summary, for  $\sigma_i = 350$  MPa ( $\sigma_i > \sigma_0$ ) the visco-plasticity during initial 3 mins of cooling is over-estimated by an order of magnitude by relaxation/creep in the range,  $996.5^\circ\text{C} \leq T \leq 998^\circ\text{C}$ . Thereafter, there is good agreement between the measured visco-plastic strain and the calculated relaxation/creep strain during subsequent cooling in the temperature interval  $987.5^\circ\text{C} \leq T \leq 996.5^\circ\text{C}$ , which is divided into the following sub-intervals in Table 4. However, during subsequent cooling in  $950^\circ\text{C} \leq T \leq 987.5^\circ\text{C}$  there is only a small variation in stress ( $238 \text{ MPa} \leq \sigma \leq 245 \text{ MPa}$ ) and in this case the relaxation/creep strains under-estimate the visco-plastic strain by an order of magnitude. As for  $\sigma_i = 280$  MPa ( $\sigma_i < \sigma_0$ ), there is good agreement between the measured visco-plastic strain and the calculated relaxation strain only in the initial stages of cooling in the temperature interval  $990^\circ\text{C} \leq T \leq 996^\circ\text{C}$ . On further cooling in  $950^\circ\text{C} \leq T \leq 994^\circ\text{C}$  the stress progressively increases and visco-plasticity becomes negligible (uncertainty in strain measurements = 50 micro-strain =  $5 \times 10^{-5}$  and therefore strains below this threshold have to be ignored). In this case, the creep strain initially over-estimates the visco-plastic strain in the temperature range,  $980^\circ\text{C} \leq T \leq 994^\circ\text{C}$ , but thereafter in the temperature range,  $950^\circ\text{C} < T < 960^\circ\text{C}$  creep/relaxation is absent, which is consistent with the absence of visco-plastic strain on cooling.

#### 4. Discussion



During cooling, the thermal strain is accommodated by an elastic and visco-plastic contribution. Visco-plasticity during cooling arises from stress relaxation/creep. Both creep and relaxation are time dependent processes and although the micro-mechanisms are similar, some differences exist [35]. From the isothermal loading tests it was observed that both creep rate and the relaxation rate data could be represented by a power-law fit in the temperature range of 950 – 1000°C. The acquisition time for a given neutron diffraction measurement was 3 mins. An increasing acquisition time results in greater fidelity of the reading for lattice spacing, but this increasing time interval will fail to capture the transient stress/strain evolution during cooling. Specifically, in the isothermal relaxation tests and corresponding to the time interval of 3 mins, the uncertainty in (200) lattice strain,  $\Delta\epsilon^{200}$  is about  $5 \times 10^{-5} \ll \Delta\epsilon^{rel}$ . Further, within this time interval, the decrease in relaxation strain rate from 1000°C to 950°C for a given  $\sigma/\sigma_0$  is three-fold. Also, the decrease in creep strain rate from 1000°C to 950°C is three-fold for  $\sigma/\sigma_0 < 0.92$ , but increases rapidly for increasing  $\sigma/\sigma_0$ .

It is therefore reasonable to apply the relaxation strain rate measured at 950°C to the temperature interval,  $950^\circ\text{C} \leq T \leq 960^\circ\text{C}$  and similarly that measured at 1000°C to the temperature interval,  $980^\circ\text{C} \leq T \leq 1000^\circ\text{C}$ , while accepting the fact that the relaxation strain could be slightly over-estimated closer to 980°C. For  $\sigma/\sigma_0 \leq 0.92$ , it is reasonable to adopt a similar approach as in the case of the relaxation rate for the applicability of the creep rate in the two above-mentioned temperature ranges. Some comments can now be made with respect to the calculated relaxation/creep strain with the measured visco-plastic strain during cooling.

In the calculation of the evolution of stress and strain during cooling an elementary 1D approach was adopted, where the length of the sample is fixed ( $\Delta\epsilon = 0$ ) and all of the thermal strain was accommodated elastically and visco-plastically. This approach was shown to be valid, since the visco-plastic strain calculated from evolution of the axial stress during

cooling ( $\Delta\sigma/E$ ) was equal to the directly measured (200) micro-strain from the changes in d-spacing of the (200) lattice planes. In this case, all the samples were seeded such that the axial orientation of the bars were within  $5^\circ$  from [100], i.e. the (200) planes were oriented near-normal to the applied stress. The time interval for neutron data acquisition was 3 mins and for a given cooling rate determines the temperature interval,  $\Delta T$  within which the visco-plastic strain is measured. When this is coupled with stress/relaxation creep, some important points should be noted. When  $\sigma/\sigma_0 > 1$  ( $\sigma_i = 350$  MPa), appreciable visco-plasticity is observed within initial 3 mins of cooling;  $998^\circ\text{C} \leq T \leq 996.5^\circ\text{C}$ , and relaxation/creep strain significantly over-estimates this visco-plasticity. Unlike for  $\sigma/\sigma_0 < 1$ , there is a marked time-dependence of relaxation/creep strain rate in the isothermal tests when  $\sigma/\sigma_0 > 1$ . Therefore, the given time interval is unable to capture the transient effects if the power law equation for relaxation/creep (c.f. Table 4), which is used in conjunction with Equation 4. Consequently a smaller time interval  $\Delta t_i \ll 3 \text{ mins}$  is required to accurately calculate the contribution of relaxation/creep to visco-plasticity during initial cooling. The relaxation/creep during initial 3 mins of cooling is then given by,  $\Delta\epsilon^{\text{rel/creep}} = \sum \epsilon(\dot{\epsilon})\Delta t_i = \int_0^{\Delta t} \dot{\epsilon}(t)dt$  and  $\Delta t = \sum \Delta t_i = 3 \text{ mins}$ .

However, it is not possible to indefinitely decrease the time interval for calculation. A lower acquisition time leads to greater measurement uncertainties and therefore an upper bound exists for the time/temperature interval for calculations. During subsequent cooling in the temperature range,  $987.5^\circ\text{C} \leq T \leq 996.5^\circ\text{C}$ , relaxation/creep adequately accounts for visco-plasticity during cooling (and is an order of magnitude greater than the uncertainty in measurement of strain,  $\Delta\epsilon_{200} \approx 5 \times 10^{-5}$ ) thereby indicating the validity of the approach. It is also important to emphasise that in this calculation the time interval for measurement does not significantly bias the results, as summarised in Table 6 for an increase in time interval for the calculations. On the other hand for when  $\sigma/\sigma_0 < 1$ , ( $\sigma_i = 280$  MPa), the visco-plastic strain

during initial cooling,  $990^{\circ}\text{C} \leq T \leq 996^{\circ}\text{C}$  is comparable to the relaxation strain obtained from isothermal tests. Like in the previous case, the time interval for measurement does not significantly bias the results, as summarised in Table 7.

It follows from the preceding discussion that the visco-plastic strain during cooling for a nominal cooling rate of  $1^{\circ}\text{C/s}$  is well accounted for by relaxation/creep obtained from the isothermal loading tests and corresponding to a time interval of 3 mins. On the other hand, at lower temperatures when the visco-plastic strain measured during cooling is compared with that calculated from the isothermal loading tests, there are some discrepancies that are observed. These can be explained as follows. When  $\sigma/\sigma_0 > 1$  ( $\sigma_i = 350$  MPa), dominant visco-plasticity occurs through stress relaxation/creep. A reduction in barriers for dislocation motion from thermally activated processes such as climb and cross-slip results in increased dislocation glide and mobility. This occurs within  $\gamma$ -channels as well as in  $\gamma'$  precipitates, where in the latter stacking faults have been observed [31]. It can be inferred that the elimination of such barriers to dislocation motion persist to lower temperatures as well, since on further cooling in the range,  $957^{\circ}\text{C} \leq T \leq 987.5^{\circ}\text{C}$ , all of the thermal strain is accommodated by relaxation/strain and the stress is constant,  $\sigma \approx 245$  MPa. However, such a “history” dependence of the microstructure during cooling from higher temperature because of the accompanying relaxation/creep to lower temperatures cannot arise in the isothermal loading tests. Therefore, it is not unexpected that the stress relaxation/creep calculated for these lower stresses in the isothermal tests under-estimates the extent of visco-plasticity during cooling. On further cooling in the temperature range;  $900^{\circ}\text{C} \leq T \leq 957^{\circ}\text{C}$ , no further visco-plasticity is observed leading to stress build-up where all the thermal strain is accommodated elastically;  $\alpha\Delta T = \frac{\Delta\sigma}{E} \approx 6.5 \times 10^{-4}$ . When  $\sigma/\sigma_0 < 1$  ( $\sigma_i = 280$  MPa), the initial visco-plasticity that occurred through stress relaxation in the range,  $990^{\circ}\text{C} \leq T \leq 996^{\circ}\text{C}$ , was subsequently absent on further cooling (i.e.  $\Delta\varepsilon^{\text{vp}} < 5 \times 10^{-5} =$

measurement uncertainty) in the range,  $950^{\circ}\text{C} \leq T \leq 990^{\circ}\text{C}$ . However in the range,  $980^{\circ}\text{C} \leq T \leq 990^{\circ}\text{C}$ , stress relaxation from isothermal tests was  $\sim 10^{-4}$  and therefore over-estimating the visco-plasticity during cooling. In this case, it can be inferred that modifications to the dislocation density arising during initial stress relaxation, where elastic strain is converted into plastic strain plays a significant role in subsequently retarding relaxation on further cooling. Like in the preceding case, the changing dislocation density from prior relaxation plays a significant role on subsequent relaxation during cooling, which will not be captured in the isothermal loading tests.

Following from this discussion, there are some important aspects that need careful attention during the computational modelling of solidification in Ni-base alloys. Specifically in lieu of this study when stress relaxation/creep is used to calculate visco-plasticity for describing the evolution of stress/strain in the temperature range of  $900 - 1000^{\circ}\text{C}$ . First, when the initial stresses are high ( $\sigma/\sigma_0 > 1$ ), visco-plasticity is dominant and there is a larger temperature range over which this approach can be used before the relaxation/creep strain under-estimates visco-plasticity. Second, when the initial stresses are low ( $\sigma/\sigma_0 < 1$ ), relaxation is less dominant and there is a very small temperature range beyond which the relaxation strain over-estimates visco-plasticity. Lastly, it must be noted that below a certain temperature, relaxation/creep strains calculated using the best-fit equations from the isothermal tests are negligible. In this case all of the thermal strain is accommodated through an increase in elastic stress and also the results agree with the directly measured visco-plastic strain during cooling.

For more accurate calculation of visco-plasticity in-situ solidification experiments must be performed, where it is possible in principle to directly measure the visco-plastic strain [37]. However, the only drawback in such cases is that the entire sample is melted and during

subsequent freezing the structure is polycrystalline. Therefore additional deformation mechanisms, such as grain boundary sliding can occur and is less representative for single crystals, which is the object of study in this article.

## **Conclusions**

- The initially applied stress plays an important role in visco-plasticity during cooling.
- It was observed that the visco-plastic response during cooling arises from stress relaxation and creep.
- Very good agreement is obtained for the visco-plastic strain measured directly from the (200) lattice planes with that calculated from the macro-stress for axial orientations close to [100].
- Modelling approaches that use such constitutive equations to calculate the evolution of stress and strain during cooling from re-heating isothermal loading tests have to be used with caution.
  - Specifically, when the initial stresses are high, there is a larger temperature range over which this approach can be used before the relaxation/creep strains begin to under-estimate the visco-plasticity during cooling.
  - For a lower initial stress there is a smaller temperature range beyond which the relaxation strains over-estimate the visco-plasticity during cooling.

## **Acknowledgements**

The authors acknowledge the help of Mr. Kevin Goodwin, Martin Perry and Dean Welton from the Precision Casting Facility (PCF) for the manufacture of the tensile test pieces and fixtures for the Instron machine. Dr. Chunlei Qiu of Cardiff University is also acknowledged for assistance in one of the experiments.

## References

- [1] C. Panwisawas, H. Mathur, J.-C. Gebelin, D. Putman, C.M.F. Rae, R.C. Reed, Prediction of recrystallization in investment cast single-crystal superalloys, *Acta. Mater.* 61 (2013) 51-66.
- [2] C. Panwisawas, J.-C. Gebelin, R.C. Reed, Analysis of the mechanical deformation arising from the investment casting of directionally solidified and single crystal superalloys, *Mater. Sci. Technol.* 29 (2013) 843 – 853.
- [3] C. Panwisawas, Modelling and Prediction of Recrystallisation in Single Crystal Superalloys, PhD Thesis, University of Birmingham, 2013.
- [4] Z.L. Li, D.D. Zhang, X.L. Su, Q.Y. Xu, B.C. Liu, Role of as-cast dendritic microstructure in recrystallization of a Ni-based single crystal superalloy, *J. Alloys Comp.* 660 (2016) 115 – 124.
- [5] Z.L. Li, Q.Y. Xu, B.C. Liu, Microstructure simulation on recrystallization of an as-cast nickel based single crystal superalloy, *Comp. Mater. Sci.* 107 (2015) 122 – 133.
- [6] D.C. Cox, B. Roebuck, C.M.F. Rae, R.C. Reed, Recrystallisation of single crystal superalloy CMSX-4, *Mater. Sci. Technol.* 19 (2003) 440-446.
- [7] Z.L. Li, X.Y. Fan, Q.Y. Xu, B.C. Liu, Influence of deformation temperature on recrystallization in a Ni-based single crystal superalloy, *Mater. Lett.* 160 (2015) 318 – 322.
- [8] R.W. Salkeld, T.T. Field, E.A. Ault, Preparation of single crystal superalloys for post-casting heat treatment. *United States Patent* 5413648 (1995).
- [9] P. Carter, D.C. Cox, C.A. Gandin, R.C. Reed, Process modelling of grain selection during the solidification of single crystal superalloy castings. *Mater. Sci. Eng. A280* (2000) 233–246.

- [10] H.N. Mathur, Recrystallisation in single crystal nickel-based superalloys, PhD Thesis, University of Cambridge, 2013.
- [11] H.N. Mathur, C.N. Jones, C.M.F. Rae, A study on the effect of composition, and the mechanisms of recrystallization in single crystal Ni-based superalloys. *MATEC Web of Conferences* 14 (2014) 07003.
- [12] L. Wang, F. Pyczak, J. Zhang, L.H. Lou, R.F. Singer, Effect of eutectics on plastic deformation and subsequent recrystallization in the single crystal nickel base superalloy CMSX-4, *Mater. Sci. Eng. A* 532 (2012) 487 – 492.
- [13] M. Dupeux, J. Henriot, M. Ignat, Tensile stress relaxation behaviour of Ni-based superalloy single crystals between 973 and 1273K, *Acta Metall.* 35 (1987) 2203 – 2212.
- [14] H. Wang, B. Clausen, C. N. Tome, P. D. Wu, Studying the stress relaxation and creep on lattice strain evolution of stainless steel under tension, *Acta Mater.* 61 (2013) 1179 – 1188.
- [15] P. Feltham, Stress relaxation in alpha-iron at low temperatures, *Phil. Mag.* 67 (6) (1961) 847 – 850.
- [16] B. Jakobson, H. F. Poulsen, U. Lienert, J. Bernier, C. Gundlach, W. Pantleon, Stability of dislocation structures in copper towards stress relaxation investigated by high angular resolution 3D X-ray diffraction, *Phys. Stat. Sol. A* 206 (2009) 21 – 30.
- [17] Z.L. Li, J.C. Xiong, Q.Y. Xu, J.R. Li, B.C. Liu, Deformation and recrystallization of single crystal nickel-based superalloys during investment casting, *J. Mater. Proc. Technol.* 217 (2015) 1-12.
- [18] J. Meng, T. Jin, X.F. Sun, Z.Q. Hu, Effect of surface recrystallization on the creep rupture properties of a nickel-base single crystal superalloy, *Mater. Sci. Eng. A* 527 (2010) 6119-6122.

- [19] J.J. Moverare, S. Johansson, R.C. Reed, Deformation and damage mechanisms during thermal–mechanical fatigue of a single-crystal superalloy, *Acta. Mater.* 57 (2009) 2266–2276.
- [20] N. Wang, S. Mokadem, M. Rappaz, W. Kurz, Solidification cracking of superalloy single- and bi-crystals, *Acta Mater.* 52 (2004) 3173 – 3182.
- [21] J.-M. Drezet, B. Mireux, Z. Szaraz, T. Pirling, In-situ neutron diffraction during casting: determination of rigidity point in grain refined Al-Cu alloys, *Materials* 7 (2014) 1165 – 1172.
- [22] J.L. Chaboche, A review of some plasticity and viscoplasticity constitutive theories, *Int. J. Plast.* 24(10) (2008) 1642–1693.
- [23] J.-B. le Graverend, J. Cormier, F. Gallerneau, P. Villechaise, S. Kruch, J. Mendez, A microstructure-sensitive constitutive modeling of the inelastic behavior of single crystal nickel-based superalloys at very high temperature, *Int. J. Plast.* 59 (2014) 55–83.
- [24] M. McLean, B.F. Dyson, Modeling the Effects of Damage and Microstructural Evolution on the Creep Behavior of Engineering Alloys, *J. Eng. Mater. Technol.* 122 (2000) 273–278.
- [25] A. Ma, D. Dye, R.C. Reed, A model for the creep deformation behaviour of single-crystal superalloy CMSX-4, *Acta. Mater.* 56 (2008) 1657 – 1670.
- [26] J. Cormier, G. Cailletaud, Constitutive modeling of the creep behavior of single crystal superalloys under non-isothermal conditions inducing phase transformations, *Mater. Sci. Eng. A* 527 (2010) 6300–6312.
- [27] J. Coakley, D. Dye, H.C. Basoalto, Creep and creep modelling of a multimodal nickel-base superalloy, *Acta. Mater.* 59 (2011) 854 – 863.
- [28] Z. Zhu, H.C. Basoalto, N. Warnken, R.C. Reed, A model for the creep deformation behaviour of nickel-based single crystal superalloys, *Acta. Mater.* 60 (2012) 4888 – 4900.



- [29] D.M. Collins, D.J. Crudden, E. Alabort, T. Connolley, R.C. Reed, Time-resolved synchrotron diffractometry of phase transformations in high strength nickel-based superalloys, *Acta Mater.* 94 (2015) 244 – 256.
- [30] D. Dye, J. Coakley, V.A. Vorontsov, H.J. Stone, R.B. Rogge, Elastic moduli and load partitioning in a single-crystal nickel superalloy, *Scr. Mater.* 61 (2009) 109 – 112.
- [31] N. D'Souza, J. Kelleher, C.L. Qiu, S.Y. Zhang, S. Gardner, R. E. Jones, D. Putman, C. Panwisawas, The role of stress relaxation and creep during high temperature deformation in Ni-base single crystal superalloys-Implications to strain build-up during directional solidification, *Acta. Mater.* 106 (2016) 322-332.
- [32] C.L. Qiu, N. D'Souza, J. Kelleher, C. Panwisawas, An experimental investigation into the stress and strain development of a Ni-base single crystal superalloy during cooling from solidification, Under review.
- [33] M. P. Jackson, M. J. Starink, R. C. Reed, Determination of the precipitation kinetics of Ni<sub>3</sub>Al in the Ni – Al system using differential scanning calorimetry, *Mater. Sci. Eng. A.* 264 (1999) 26 – 38.
- [34] M.R. Daymond, M. Preuss, B. Clausen, Evidence of variation in slip mode in a polycrystalline nickel-base superalloy with change in temperature from neutron diffraction strain measurements, *Acta Mater.* 55 (2007) 3089 – 3102.
- [35] F. A. Ackeroyd, R. L. Ashworth, S. D. Johnston, J. M. Martin, C. M. Moreton-Smith, D. S. Sivia, *OpenGenie* 1999.
- [36] J. Coakley, R. C. Reed, J. L. W. Warwick, K. M. Rahman, D. Dye, Lattice strain evolution during creep in single-crystal superalloys, *Acta Mater.* 60 (2012) 2729 – 2738.

[37] J.-M. Drezet, B. Mireux, Z. Szaraz, T. Pirling, In-situ neutron diffraction during casting: Determination of rigidity point in grain refined Al-Cu alloys, *Materials* 7 (2014) 1165-1172.

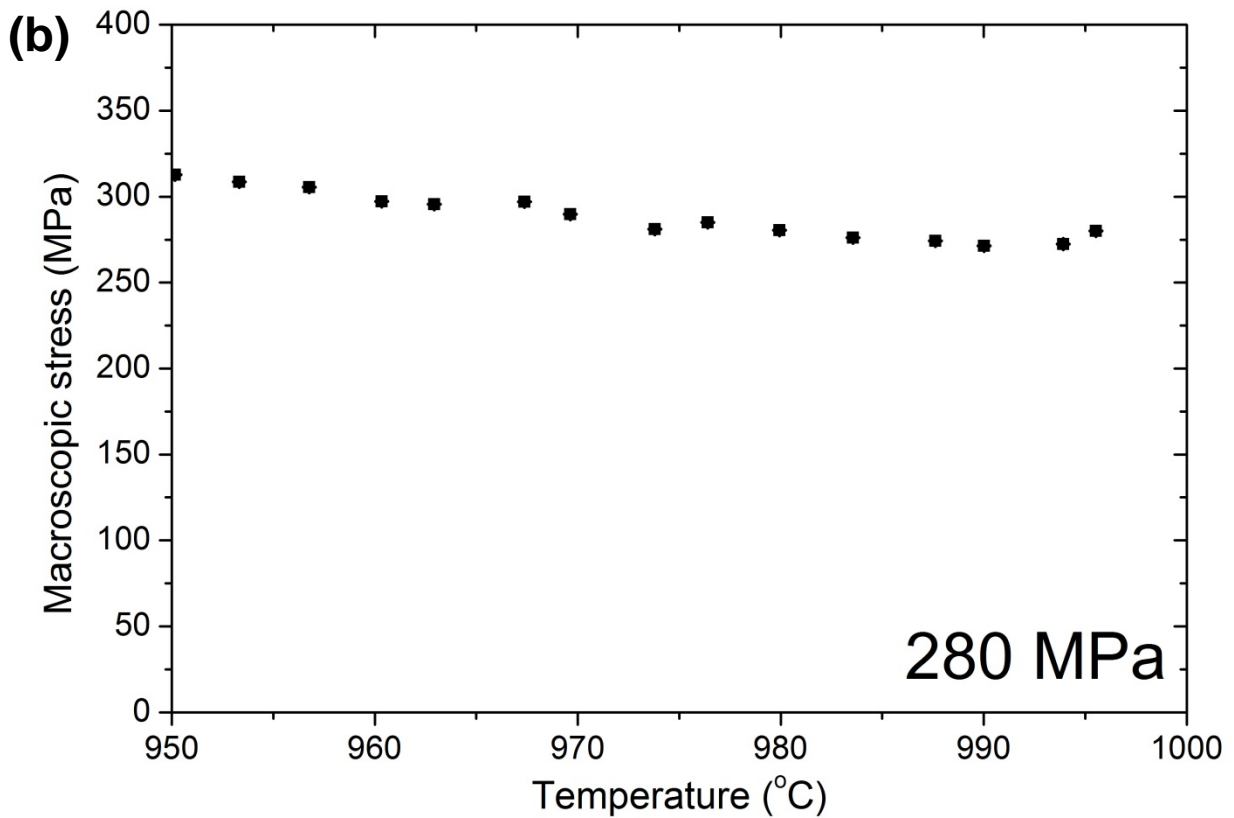
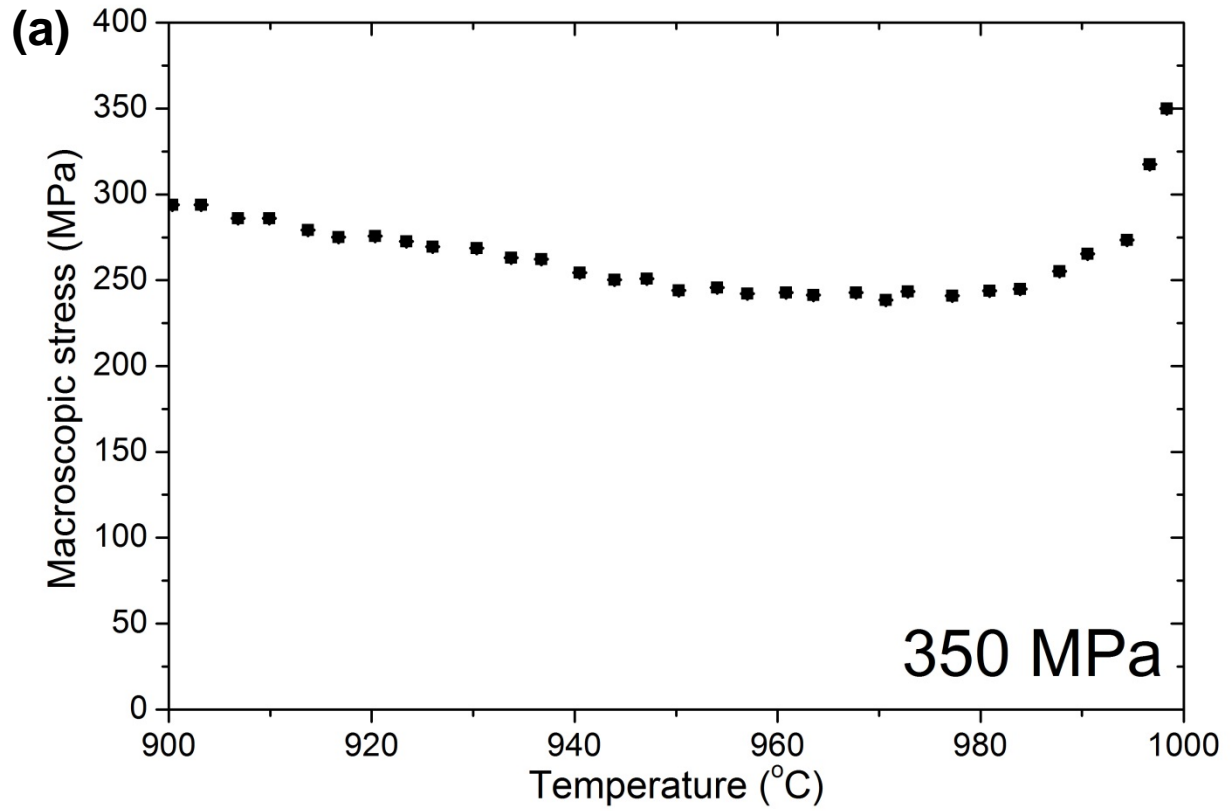


Figure 1: Macroscopic stress evolution during the in-situ cooling experiment from the initial stresses of (a) 350 MPa and (b) 280 MPa. Given the scale on the Y-axis (MPa) and the magnitude of error ( $10^{-3}$  MPa), this error bar is barely noticeable.

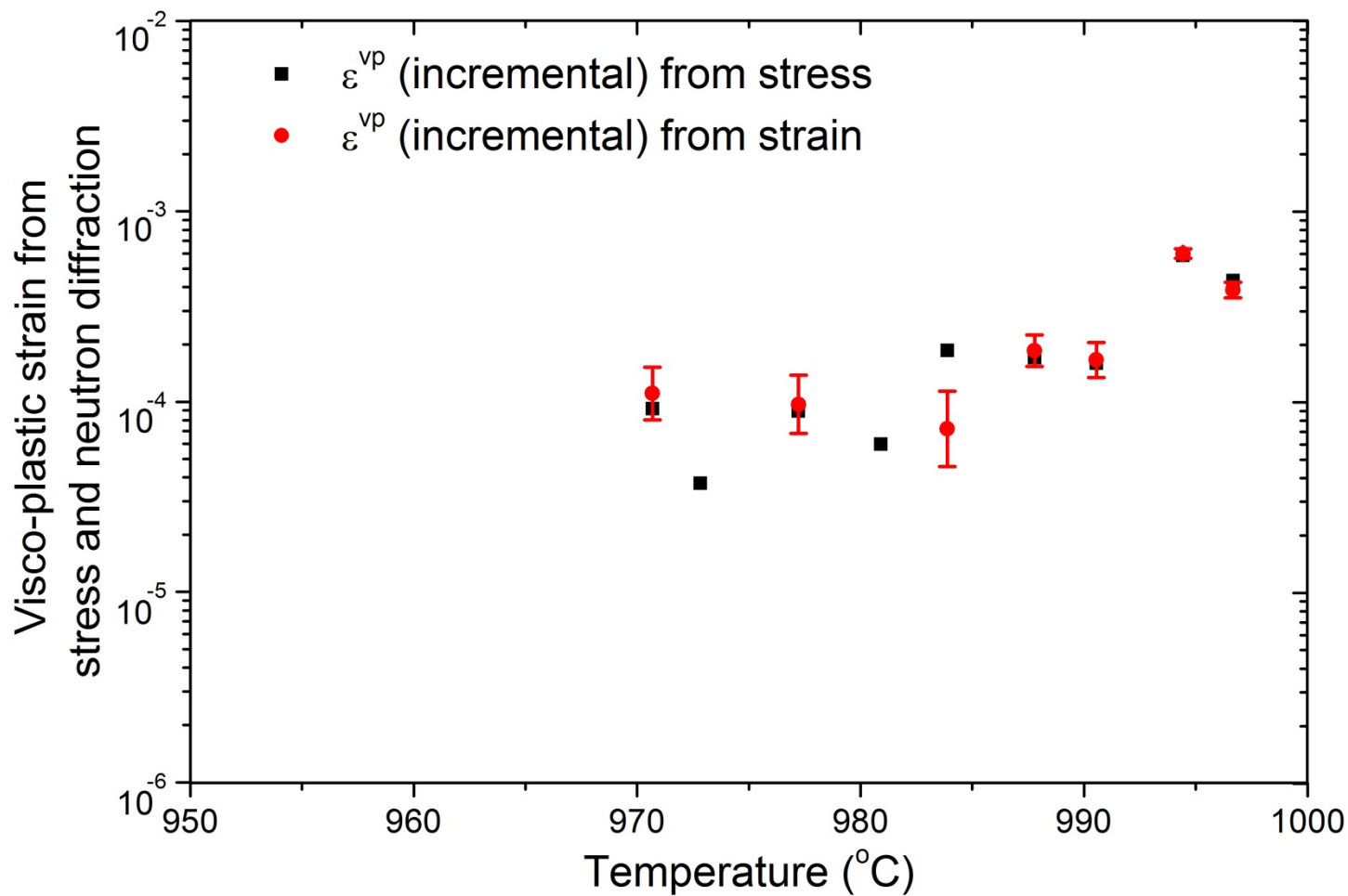


Figure 2: Comparison between the measured visco-plastic strain from macro-stress data and neutron measurement using the in-situ cooling from the initial stress of 350 MPa. There is negligible error for visco-plastic strain obtained from measured stress, c.f. Figure 1 (a).

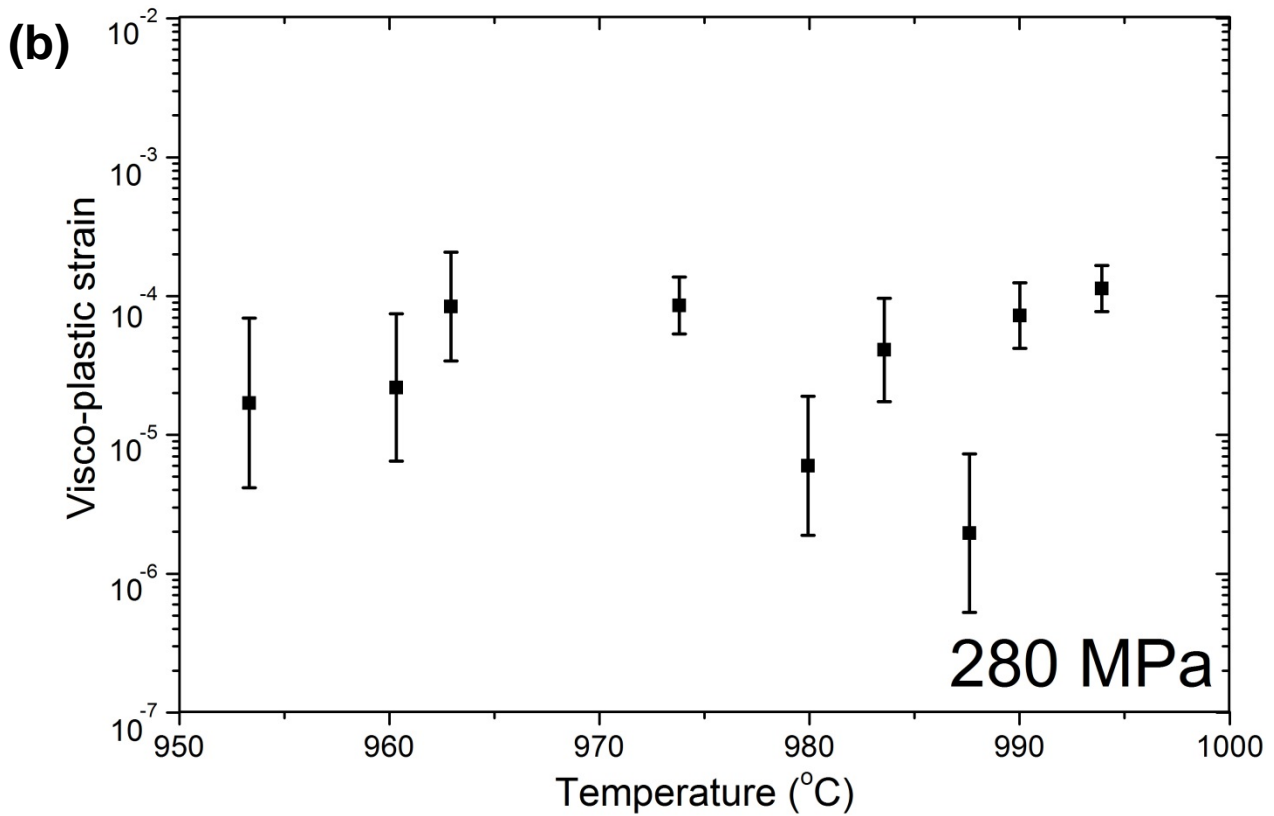
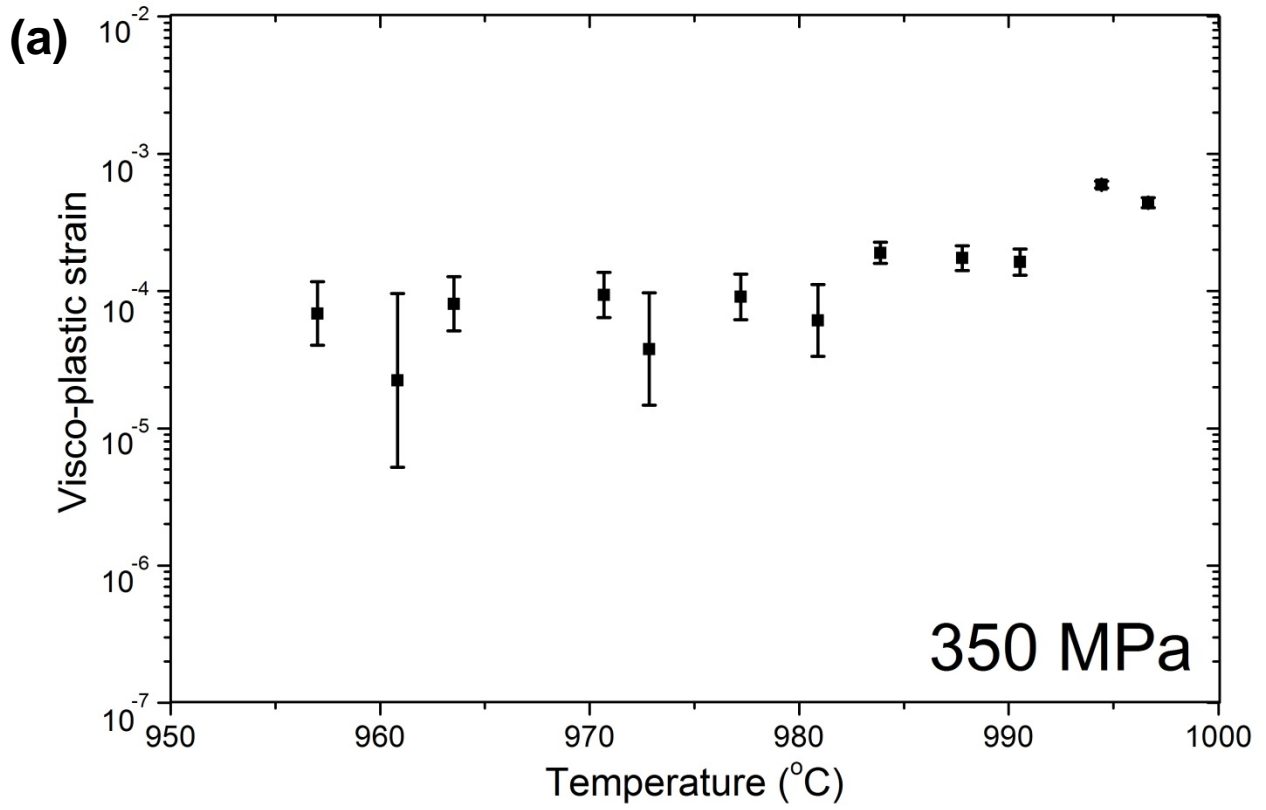


Figure 3: The evolution of visco-plastic strain during continuous cooling from the initial stress of (a) 350 MPa and (b) 280 MPa.

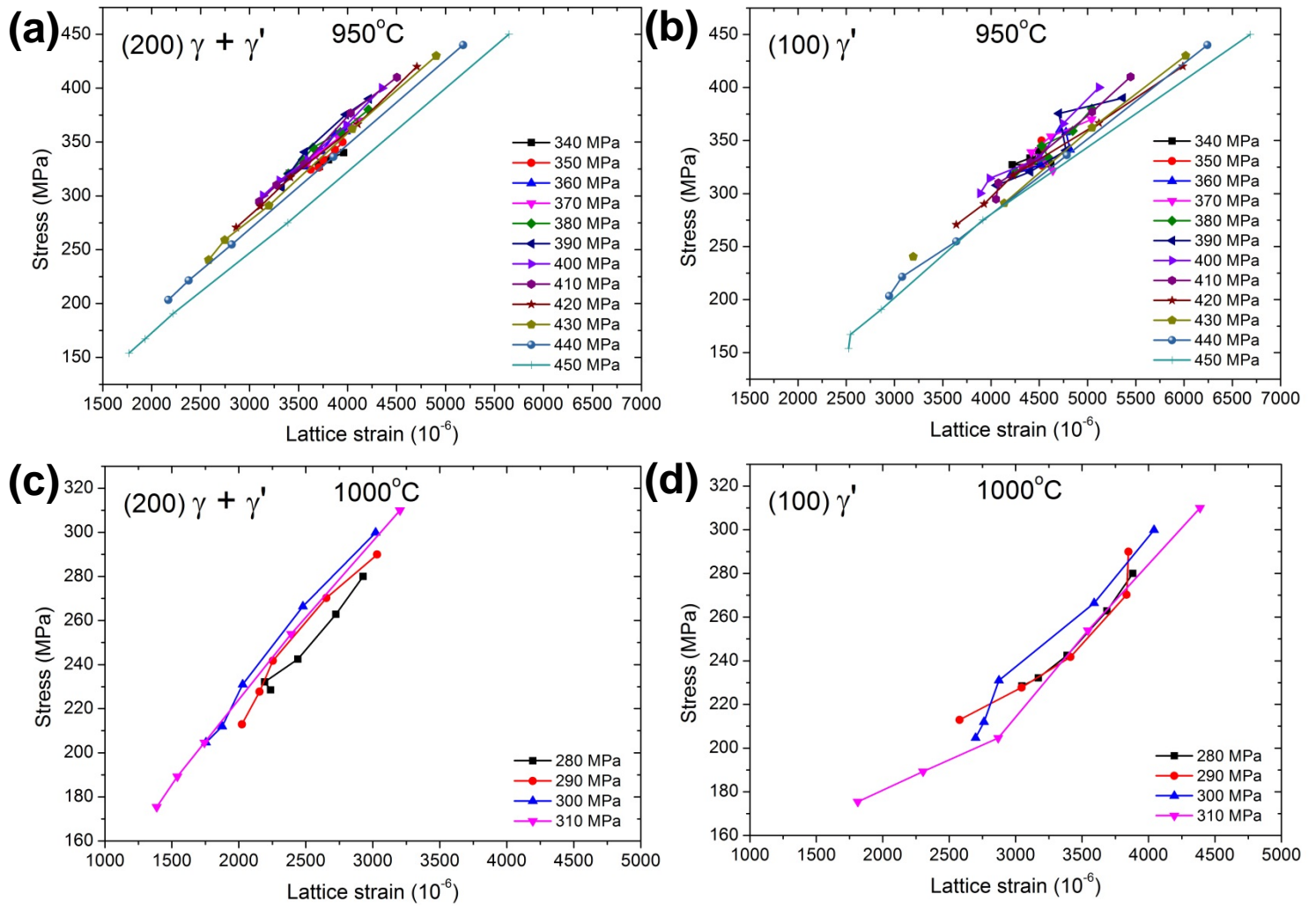


Figure 4: Axial elastic response of  $\gamma$  and  $\gamma + \gamma'$  phases during relaxation at 950°C and 1000°C under strain control measurement.

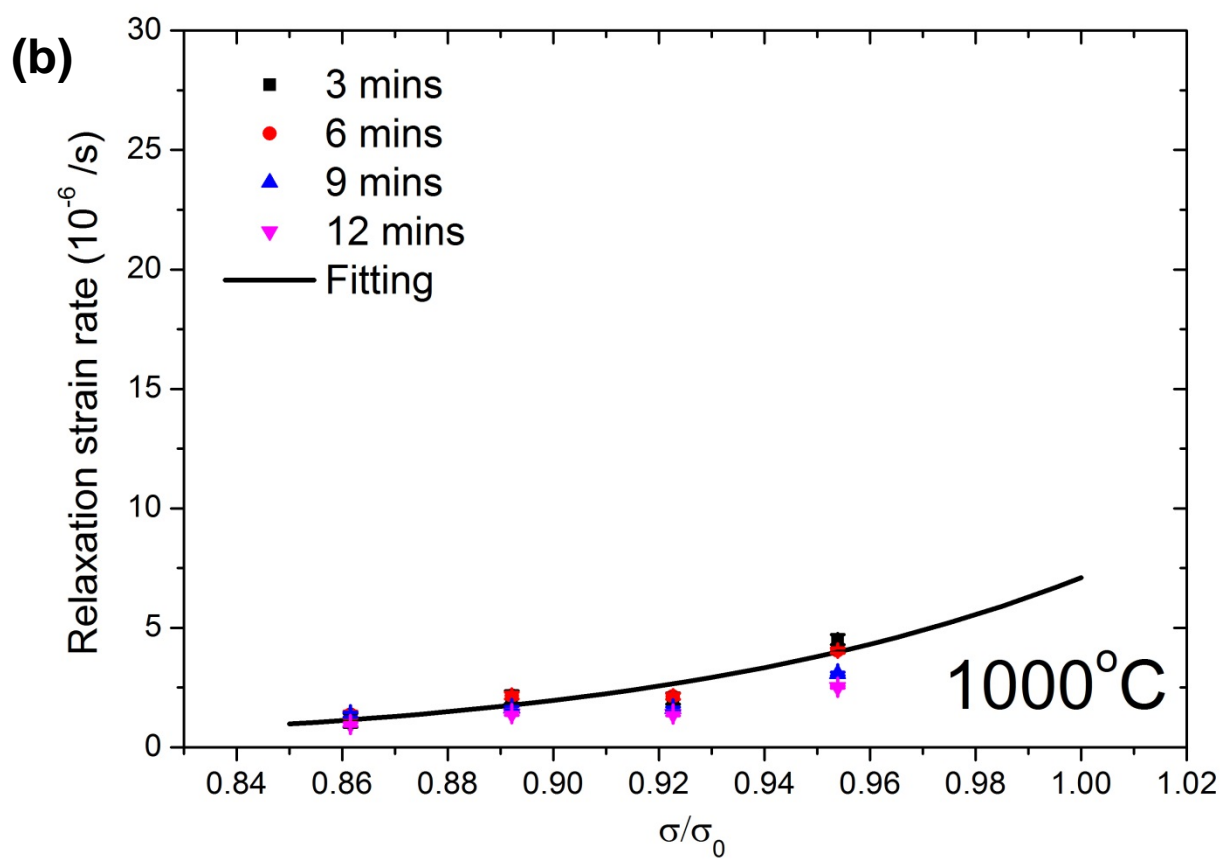
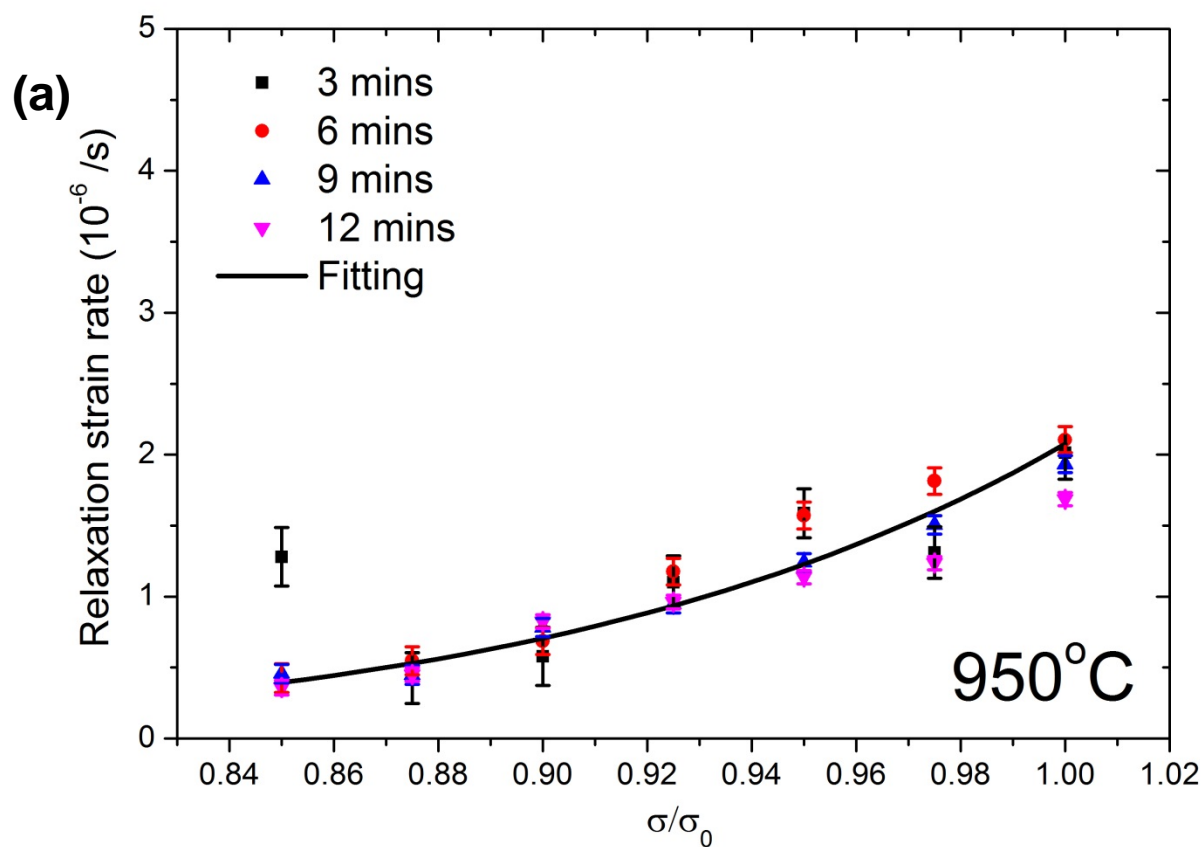


Figure 5: Dependence of the calculated and fitting relaxation strain rate on stress and time at (a) 950°C; and (b) 1000°C.

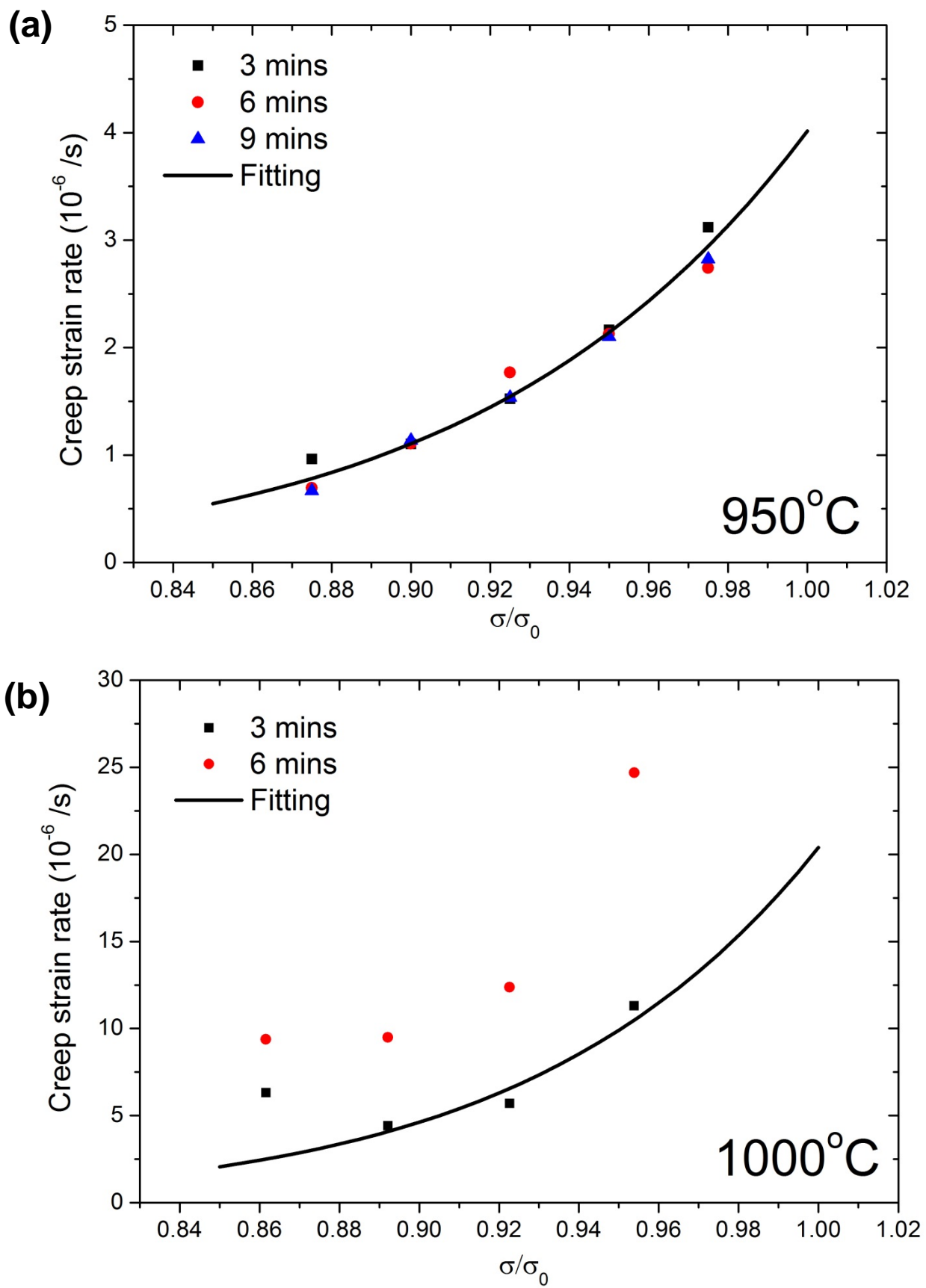


Figure 6: Dependence of the calculated and fitting creep strain rate on stress and time at (a) 950°C; and (b) 1000°C. No error bars included, as this pertains to the extensometer reading.



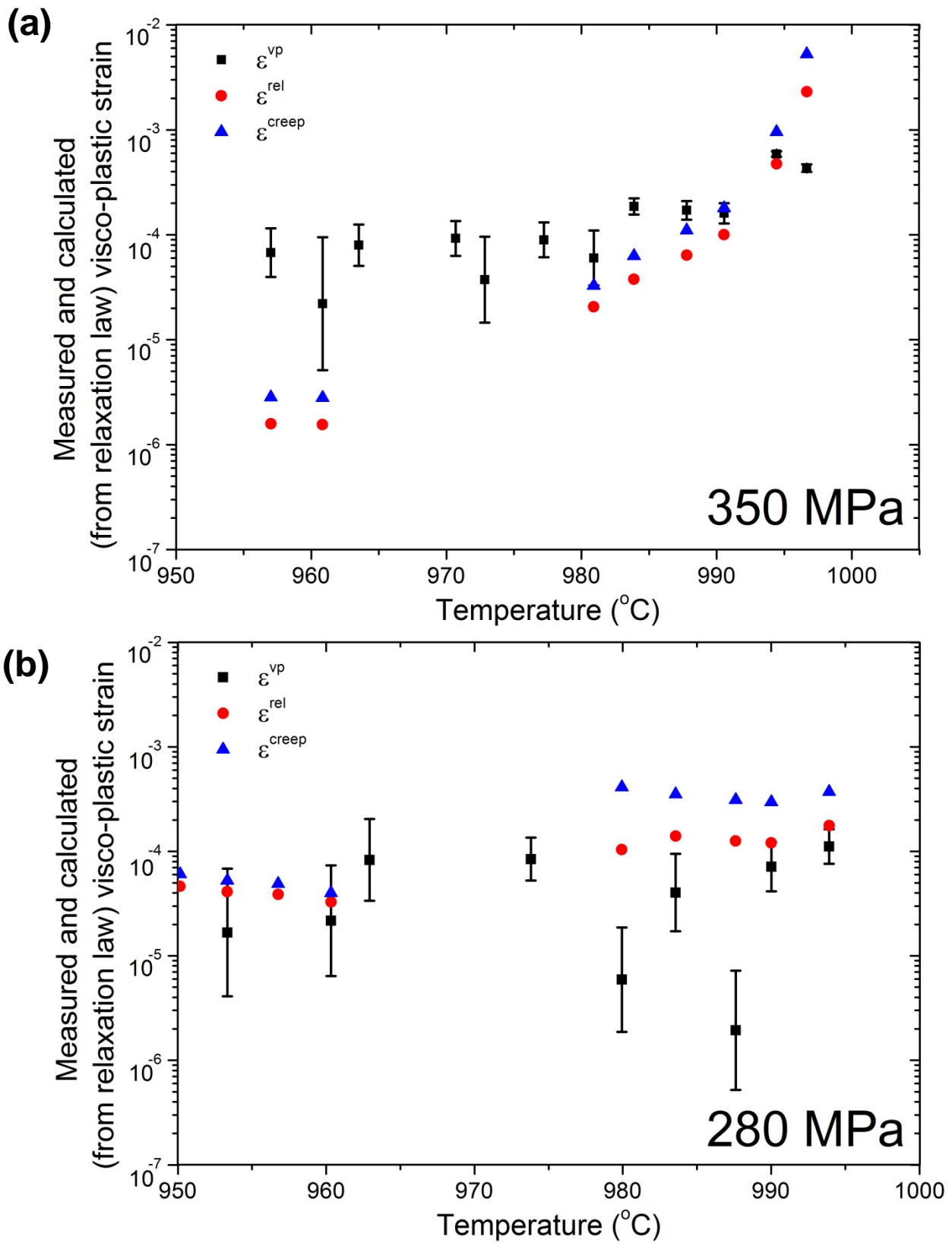


Figure 7: Comparison between the measured visco-plastic strain from macro-stress data, and calculated creep and visco-plastic strains from neutron measurement from the initial stresses of (a) 350 MPa and (b) 280MPa.

Table 1: The nominal compositions (in wt. %) of CMSX4 single-crystal superalloy.

Cr	Co	Mo	Re	W	Al	Ti	Ta	Hf	Ni
6.5	9	0.6	3	6	5.6	1	6.5	0.1	Balance

Table 2: The evolution of calculated visco-plastic strain during in-situ cooling from two initial stresses.

$\sigma_i$ (MPa)	$\Delta \epsilon^{vp}$		
	0 – 6 mins	6 – 15 mins	15 – 39 mins
<b>350</b>	$[4 - 6 \times 10^{-4}] \pm 0.35 \times 10^{-4}$	$[1 - 2 \times 10^{-4}] \pm 0.35 \times 10^{-4}$	$[0.6 - 0.9 \times 10^{-4}] \pm 0.35 \times 10^{-4}$
<b>280</b>	$[0.8 - 1 \times 10^{-4}] \pm 0.50 \times 10^{-4}$	0 (only some localised visco-plasticity between 18 to 21 mins)	

Table 3: Fitting parameters for the visco-plastic response for  $\sigma/\sigma_0 < 1$ .

T (°C)	$\dot{\epsilon}$	$\Delta t$ (mins)	A (s <sup>-1</sup> )	n
950°C	$\dot{\epsilon}^{rel}$	for all $\Delta t$	$2 \times 10^{-6}$	10.2
	$\dot{\epsilon}^{creep}$	for all $\Delta t$	$4 \times 10^{-6}$	12.3
1000°C	$\dot{\epsilon}^{rel}$	3 mins	$7 \times 10^{-6}$	12.2
	$\dot{\epsilon}^{creep}$	3 mins	$2 \times 10^{-5}$	14

Table 4: Comparison between the measured visco-plastic strain and the calculated relaxation/creep strain during subsequent cooling from 350 MPa.

Temperature interval	$\Delta \epsilon^{vp}$	$\Delta \epsilon^{rel}$	$\Delta \epsilon^{creep}$
994.5°C ≤ T ≤ 996.5°C	$5.8 \times 10^{-4} \pm 0.35 \times 10^{-4}$	$4 \times 10^{-4}$	$9.5 \times 10^{-4}$
990.5°C ≤ T ≤ 994.5°C	$1.6 \times 10^{-4} \pm 0.35 \times 10^{-4}$	$0.9 \times 10^{-4}$	$1.8 \times 10^{-4}$
987.5°C ≤ T ≤ 990.5°C	$1.7 \times 10^{-4} \pm 0.35 \times 10^{-4}$	$0.6 \times 10^{-4}$	$1.1 \times 10^{-4}$

Table 5: Comparison between the measured visco-plastic strain and the calculated relaxation/creep strain during subsequent cooling from 280 MPa.

Temperature interval	$\Delta\epsilon^{vp}$	$\Delta\epsilon^{rel}$	$\Delta\epsilon^{creep}$
$994^{\circ}\text{C} \leq T \leq 996^{\circ}\text{C}$	$1.1 \times 10^{-4} \pm 0.50 \times 10^{-4}$	$1.7 \times 10^{-4}$	$3.7 \times 10^{-4}$
$990^{\circ}\text{C} \leq T \leq 994^{\circ}\text{C}$	$0.8 \times 10^{-4} \pm 0.50 \times 10^{-4}$	$1.2 \times 10^{-4}$	$2.9 \times 10^{-4}$

Table 6: Comparison between the measured visco-plastic strain and the calculated relaxation/creep strain during subsequent cooling from 350 MPa during the 6 min time interval.

Time interval ( $\Delta t$ )	$\Delta\epsilon^{vp}$	$\Delta\epsilon^{rel}$	$\Delta\epsilon^{creep}$
6 mins ( $990.5^{\circ}\text{C} \leq T \leq 996.5^{\circ}\text{C}$ )	$7.5 \times 10^{-4} \pm 0.35 \times 10^{-4}$	$6.6 \times 10^{-4}$	$15 \times 10^{-4}$

Table 7: Comparison between the measured visco-plastic strain and the calculated relaxation/creep strain during subsequent cooling from 280 MPa during the 6 min time interval.

Time interval ( $\Delta t$ )	$\Delta\epsilon^{vp}$	$\Delta\epsilon^{rel}$	$\Delta\epsilon^{creep}$
6 mins ( $990^{\circ}\text{C} \leq T \leq 996^{\circ}\text{C}$ )	$1.9 \times 10^{-4} \pm 0.50 \times 10^{-4}$	$3.4 \times 10^{-4}$	$7 \times 10^{-4}$